Journal of Applied Polymer Science

Selective Adsorption and Degradation of Rhodamine B with Modified Titanium Dioxide Photocatalyst

Lanlan Bao, Minjia Meng, Kaiyong Sun, Weibing Li, Dexiang Zhao, Huaming Li, Minqiang He
School of Chemistry and Chemical Engineering, Jiangsu University, Zhenjiang, Jiangsu 212013, China
Correspondence to: M. Q. He (E-mail: hemq@ujs.edu.cn)

ABSTRACT: A new highly selective photocatalyst (RhB-MIP/TiO_2) was successfully prepared by surface molecular imprinting technique using rhodamine B (RhB) as template molecule. The adsorption kinetics show RhB-MIP/TiO_2 possessed fast adsorption rate, and adsorption behavior followed the pseudo-second-order kinetics. The static binding experiments revealed RhB-MIP/TiO_2 displayed strong affinity and high adsorption capacity for RhB. Moreover, the equilibrium adsorption rate of RhB-MIP/TiO_2 for RhB can be well fitted by the Langmuir isotherm model. The thermodynamics parameters indicated that the binding system of RhB-MIP/TiO_2 was endothermic and spontaneous. Compared with non-imprinted photocatalyst (NIP/TiO_2), RhB-MIP/TiO_2 exhibited excellent selectivity toward RhB, whose selectivity coefficient for RhB relative to rhodamine 6G (Rh6G) was 2.99. Selective photocatalytic degradation experiments indicated that the apparent rate constant for the photodegradation of RhB over RhB-MIP/TiO_2 is 0.0212 min^{-1}, being 216% of that over NIP/TiO_2 (0.0098 min^{-1}). Therefore, RhB-MIP/TiO_2 exhibited higher photocatalytic selectivity toward RhB. The prepared photocatalyst RhB-MIP/TiO_2 has a promising perspective in industrial wastewater treatment. © 2014 Wiley Periodicals, Inc. J. Appl. Polym. Sci. **2014**, *131*, 40890.

KEYWORDS: molecular imprinting; photocatalytic; rhodamine B; selective; TiO_2

Received 23 January 2014; accepted 13 April 2014
DOI: 10.1002/app.40890

INTRODUCTION

The generated dye pollutants from wastewaters can cause threat to the health of human beings and the surrounding environment.[1,2] Most of the dyes are highly toxic, carcinogenic, and reduce the light penetration in aqueous systems.[3] The biological treatment methods do not work efficiently because of the structure and stability of the dyes. It is required to develop faster treatment processes to control their pollution. Nowadays, some approaches such as coagulation/flocculation,[4] chemical precipitation,[5] membrane filtration,[6] ion-exchange,[7] adsorption,[8] and photocatalytic degradation[9] have been developed to remove the dye pollutants from wastewaters. Among them, photocatalytic degradation has attracted widespread attention due to its low cost, simplicity, high efficiency, and low secondary pollution. Titanium dioxide (TiO_2) has proven to be an efficient photocatalyst and its photocatalysis has been well-studied for environmental protection.[10–12] However, it is as yet difficult to realize selective removal of low-level targeted pollutants in the presence of other pollutants at high levels owing to the reactivity of the hydroxyl radical is difficult to control. When applied to environmental treatment, the photocatalysis may not be efficient if it aims to remove all pollutants by itself.[13] In recent years, several technologies have been proposed to enhance the selectivity of TiO_2, such as control of surface electric charge by adjusting pH,[14] modification of TiO_2 surface with specific molecules,[15] synthesis of double-region-structured photocatalyst,[16] and using molecularly imprinted polymers (MIPs),[17] among which, imprinted modification of TiO_2 is a promising way to realize selective removal of targeted pollutants.

Molecular imprinting technique (MIT) is a convenient and powerful technique to synthesize MIPs which provides artificial receptor-like binding sites for various target molecules.[18–21] MIPs have been extensively studied owing to their molecular recognition ability, specific adsorption, and wide applications in separation,[22] solid-phase extraction,[23] reactive catalysis,[24] and sensors.[25] Compared with conventional MIPs, the surface molecularly imprinted polymers (SMIPs) process more accessible sites, faster mass transfer, and higher recognition and binding ability for template molecules.[26–28] Hence, the surface of TiO_2 photocatalyst coated with imprinted layer by surface molecularly imprinted technique (SMIT), the imprinted layer, having molecular recognition ability, enables the photocatalyst to possess high selectivity toward the photodegradation of target dye pollutant.

Rhodamine B (RhB) is one of the most important dyes, which is widely used as a colorant in textiles and food stuffs. RhB is

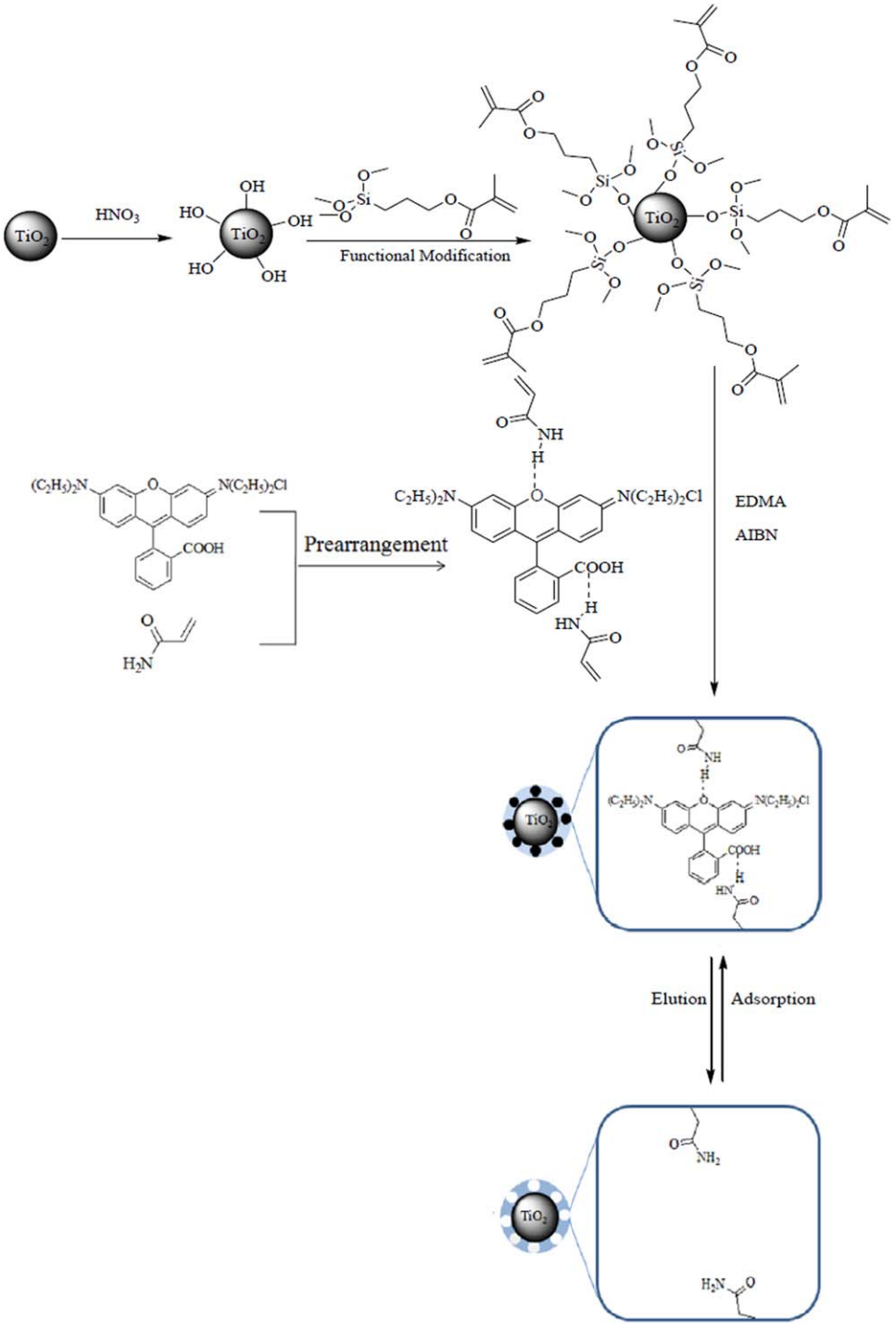

Figure 1. Schematic illustration for synthesis of RhB-MIP/TiO_2. [Color figure can be viewed in the online issue, which is available at wileyonlinelibrary.com.]

verified to be toxic and carcinogenic, and its biological degradation is slow. At present, a number of methods such as Fenton-based oxidation,[29] photocatalytic degradation,[30] sonochemical degradation,[31] and ozonationn[32] have been reported for treating RhB from wastewaters. However, the selectivity of above methods toward the RhB is very poor. Therefore, it is important to find a way to selectively remove the targeted RhB from wastewaters. To our knowledge, there are few reports on selective photocatalytic degradation for RhB using highly selective photocatalyst.

In this study, a new highly selective photocatalyst (RhB-MIP/TiO_2) with high performance for recognizing RhB was prepared by adopting the SMIT using TiO_2 as carrier material, acrylamide (AM) as functional monomer, and RhB as template molecules,

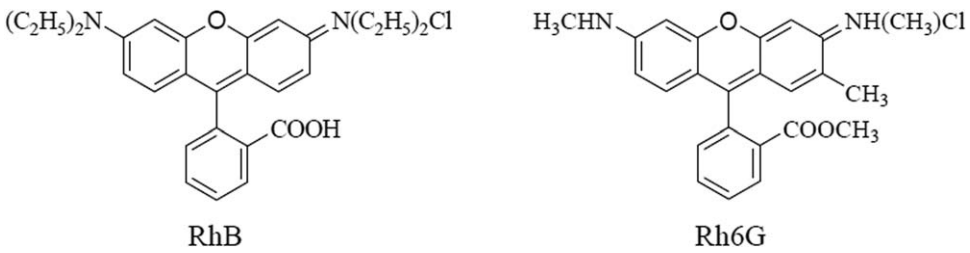

Figure 2. The structures of RhB and Rh6G.

respectively. The as-prepared RhB-MIP/TiO_2 not only exhibits high adsorption capacity and selectivity for RhB, but also can improve photocatalytic selectivity. The binding characteristics of the RhB-MIP/TiO_2 were explored using batch mode binding experiments. The thermodynamics parameters were also studied. In addition, the binding selectivity and selective degradation activity of RhB-MIP/TiO_2 toward RhB were explored in detail.

EXPERIMENTAL

Materials and Instruments

TiO_2 nanoparticles (Anatase, 20–30 nm particle size) were provided by River Hai Nami Technology Co., Ltd. (Taizhou, Jiangsu, China). Ethylene glycol dimethacrylate (EDMA) was purchased from Shanghai Haiqu Chemical Co., Ltd. (Shanghai, China). 3-Methacryloxypropyltrimethoxysilane (KH-570) was obtained from Jiangsu Chenguang Co., Ltd. (Zhengjiang, Jiangsu, China). 2,2′-Azobisisobutyronitrile (AIBN) was purchased from Shanghai NO.4 reagent & H. V. Chemical Co., Ltd. (Shanghai, China). Methanol (MeOH), acetic acid (CH_3COOH), acetonitrile (ACN), AM, methacrylic acid (MAA), 2-vinylpyridine (2-Vpy), and RhB were obtained from Shanghai Sinopharm Chemical Co., Ltd. (Shanghai, China). Rhodamine 6G (Rh6G, 98%) was purchased from Shanghai Maikun Chemical Co., Ltd. (Shanghai, China).

The instruments used in this study were as follows: SHZ-82 constant temperature bath oscillator (Zhongda Instrument, Jiangsu, China), UV-2450 Ultraviolet-visible spectrophotometer (Shimadzu, Japan), KQ2200DB ultrasonic cleaner (Kunshan Ultrasonic Instrument Co., Jiangsu, China), YXJ-II high-speed centrifuge (Zhongda Instrument, Jiangsu, China), Fourier transform infrared spectra (FTIR) (Nicolet, America), X-ray diffraction (XRD) measurements were performed on a Philips X' pert MPD Pro X-ray diffractometer using Cu Kα radiation ($\lambda = 1.5406$ Å). Transmission electron microscope was recorded with a JEOL-IEM-200CX microscope. ^{1}H-NMR spectra were recorded on a Bruker DMS-400 spectrometer (Bruker, Bremerhaven, Germany).

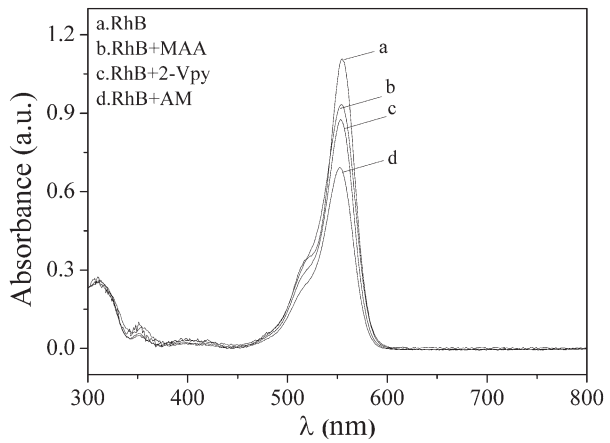

Figure 3. Adsorption spectra of the RhB in the presence of various functional monomers in ACN.

Preparation of Selective Photocatalyst RhB-MIP/TiO_2

TiO_2 nanoparticles were activated by baking for 12 h and etched with 69% HNO_3 solution by soaking in a beaker for 24 h at 25°C. Finally, the activated TiO_2 was dried under vacuum at 80°C.

Dried activated TiO_2 (2.0 g) were dispersed in water and used 5 wt % acetic acid adjusted solution to pH = 4.0. Then, KH-570 (0.4 g) was added into the above mixture. The reaction was carried at 80°C for 4 h under the atmosphere of nitrogen with continuous stirring. The products were then separated from the mixture via centrifugation and washed with methanol and water. The modified TiO_2 nanoparticles (MPS-TiO_2) were dried under vacuum at 80°C for 24 h.

The template RhB (0.5 mmol) and the functional monomer AM (2.0 mmol) were dissolved in ACN (15 mL) in a glass vial. After shaking for 6 h, MPS-TiO_2 (0.2 g), EDMA (10.0 mmol) as the cross linking agent, and AIBN (0.02 g) as the initiator were added to the solution. The mixture were fully stirred at room temperature for 4 h, followed by purging thoroughly with nitrogen for 15 min, and then sealed under vacuum. The polymerization was started by thermal initiation in a water bath at 60°C for 24 h. The product particles were washed repeatedly with a mixed solvent of methanol and acetic acid (V_{MeOH} : $V_{CH3COOH}$ = 9:1) to remove the template RhB and the remaining monomer. The selective photocatalyst (RhB-MIP/TiO_2) was obtained by centrifugation and drying. As a control, the non-selective photocatalyst (NIP/TiO_2) were prepared in the absence of the template RhB and treated with the same method. The schematic illustration for synthesis of RhB-MIP/TiO_2 is shown in Figure 1.

Binding Experiments in Dark

Batch Mode Binding Experiments. The adsorption kinetics behavior of RhB-MIP/TiO_2 for RhB was first measured. RhB-MIP/TiO_2 (10 mg) was taken in RhB aqueous solution (10 mL, 0.2 μmol/mL). The mixture was agitated in a shaken bed. After an interval of time, the mixture was centrifuged, and the

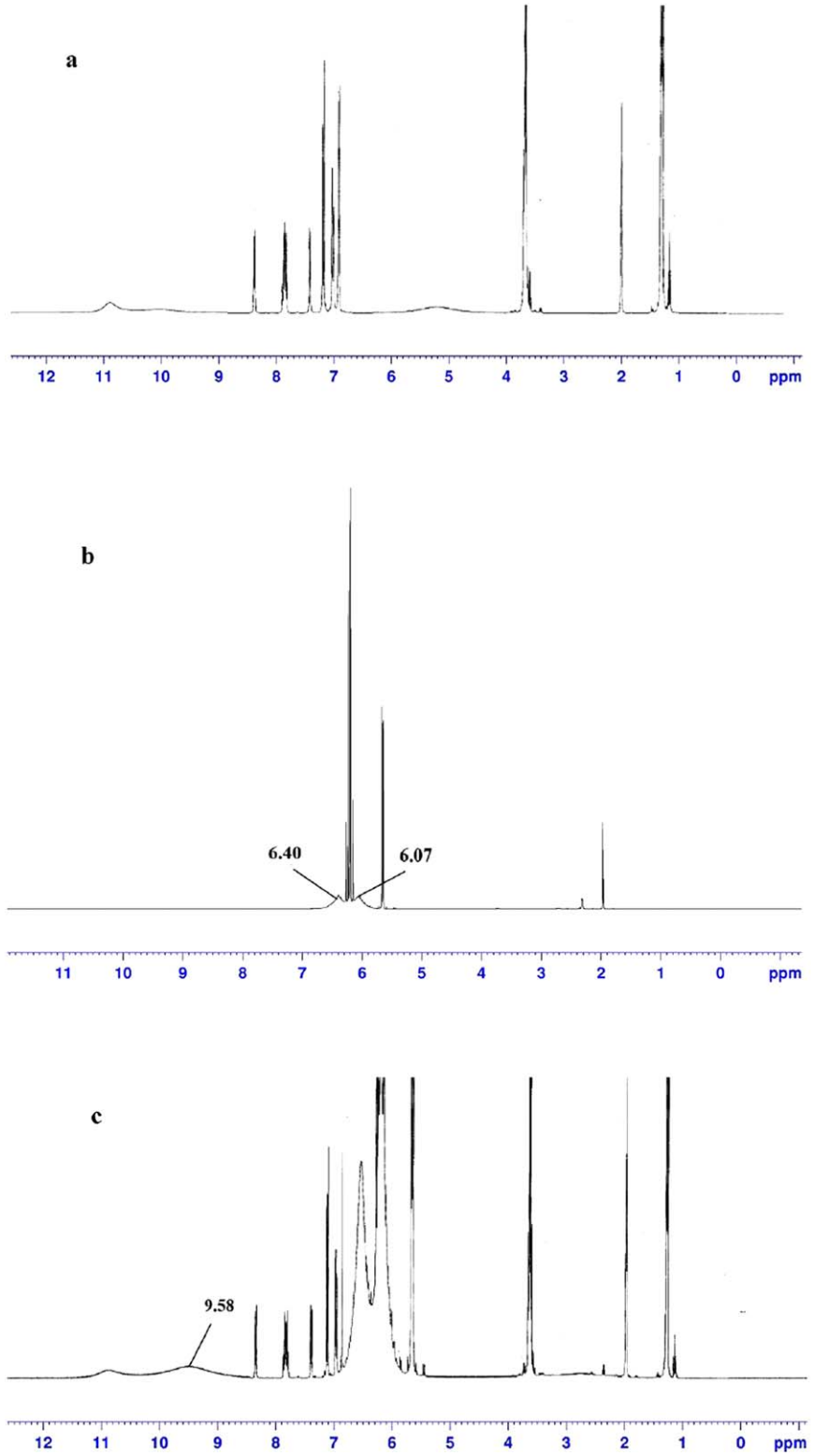

Figure 4. ^{1}H-NMR spectra of: (a) RhB, (b) AM, (c) RhB+AM in CD_3CN. [Color figure can be viewed in the online issue, which is available at wileyonlinelibrary.com.]

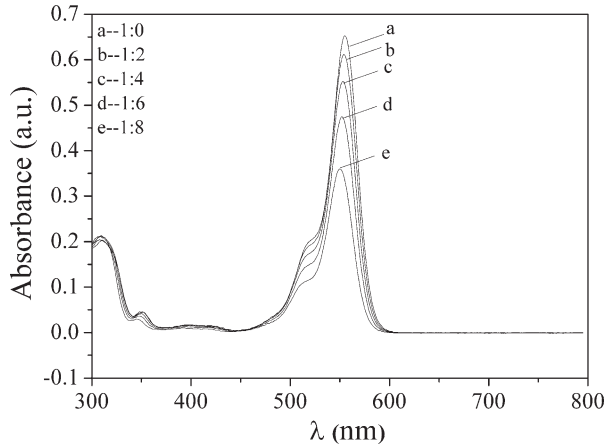

Figure 5. Adsorption spectra of the RhB in the presence of various concentration of AM in ACN.

supernatant solution was collected and diluted with water to a certain times. Finally, the concentration of RhB was determined by UV–vis spectrophotometer at 553 nm. The adsorbed amount (Q, μmol/g) was calculated by the following eq. (1).

$$Q = \frac{(C_0 - C_t)V}{W} \quad (1)$$

where W(g) is the weight of the RhB-MIP/TiO_2, V (L) is the volume of solution, C_0(μmol/L) and C_t (μmol/L) are the initial concentration of RhB and the concentration of RhB at the time t, respectively.

Adsorption isotherm of RhB-MIP/TiO_2 for RhB was determined in batch mode, RhB-MIP/TiO_2 or NIP/TiO_2 (10 mg) was taken into a centrifuge tube and then RhB aqueous solution (10 mL) with different concentrations was added. The centrifuge tubes were agitated in a shaken bed. After reaching the adsorption equilibrium, the mixture was centrifuged, and the supernatant solution was collected and diluted with water to a certain times. Finally, the concentration of RhB was determined by UV–vis spectrophotometer. The equilibrium adsorbed amount (Q_e, μmol/g) was calculated by the following eq. (2).

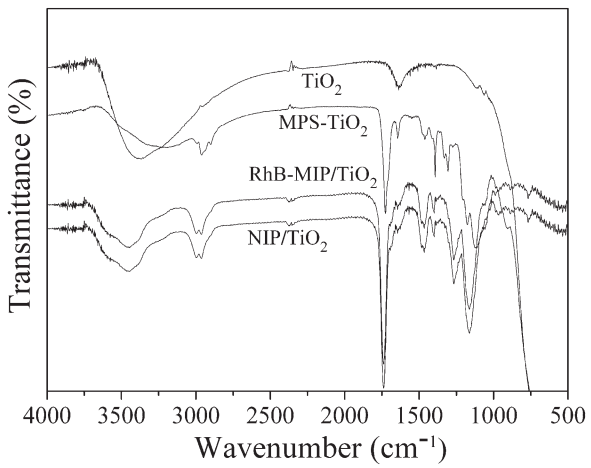

Figure 6. FTIR spectra of TiO_2, MPS-TiO_2, RhB-MIP/TiO_2, and NIP/TiO_2

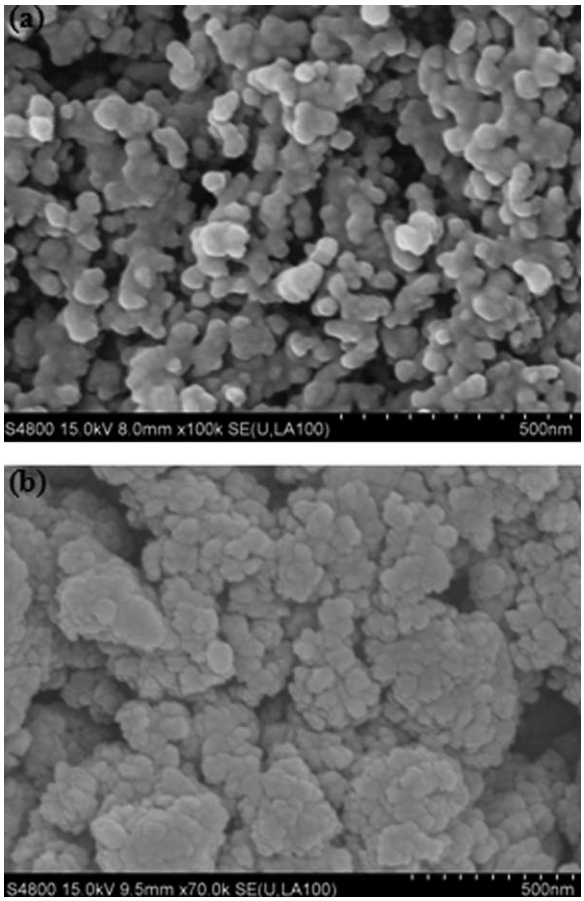

Figure 7. SEM images of: (a) TiO_2, (b) RhB-MIP/TiO_2.

$$Q_e = \frac{(C_0 - C_e)V}{W} \quad (2)$$

where W (g) is the weight of RhB-MIP/TiO_2 or NIP/TiO_2, V (L) is the volume of the solution, C_0(μmol/L) and C_e(μmol/L) are the initial concentration and the equilibrium concentration of RhB, respectively.

The binding parameters of RhB-MIP/TiO_2 are mainly estimated by Scatchard analysis with the data of static binding experiment. Scatchard equation is described by eq. (3).

$$\frac{Q_e}{C_e} = \frac{(Q_{max} - Q_e)}{K_d} \quad (3)$$

where K_d (μmol/mL) is the equilibrium dissociation constant, C_e (μmol/mL) is the equilibrium concentrations of RhB, Q_{max} (μmol/g) and Q_e (μmol/g) are the apparent maximum adsorbed amount and the equilibrium adsorbed amount of RhB, respectively.

Selective Recognition Experiments. To investigate the selectivity of RhB-MIP/TiO_2 and NIP/TiO_2 for RhB, rhodamine 6G (Rh6G) is selected as competitive substances. The size and structure of Rh6G are quite analogous to RhB. The adsorbed amount of RhB-MIP/TiO_2 or NIP/TiO_2 for RhB and the competition species Rh6G were calculated as above. The structures of RhB and Rh6G are shown in Figure 2.

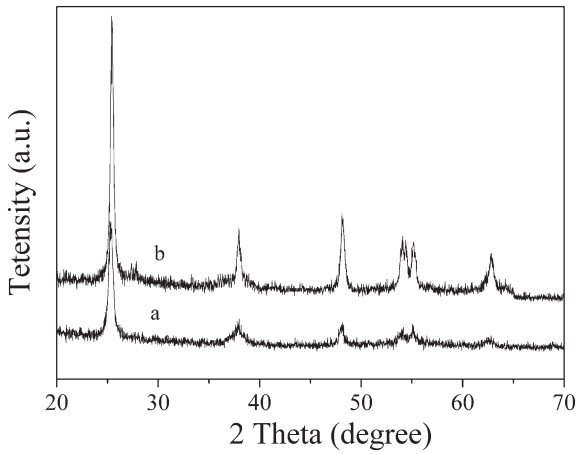

Figure 8. XRD patterns of: (a) TiO_2 and (b) RhB-MIP/TiO_2.

The distribution coefficient for RhB and Rh6G was calculated according to eq. (4).

$$K_D = Q_e / C_e \tag{4}$$

where K_D (mL/g) represents the distribution coefficient, Q_e (μmol/g) is the equilibrium adsorbed amount, and C_e (μmol/mL) is the equilibrium concentration.

The selectivity coefficient of RhB-MIP/TiO_2 or NIP/TiO_2 for RhB relative to the competition species was evaluated by α, which can be defined by eq. (5).

$$\alpha = \frac{K_{Di}}{K_{Dj}} \tag{5}$$

where α is competitive coefficient, i and j represent the template and competition species, respectively.

A relative selectivity coefficient α' can be defined by eq. (6).

$$\alpha' = \frac{\alpha_{MIP}}{\alpha_{NIP}} \tag{6}$$

where α_{MIP} and α_{NIP} are selectivity coefficient of RhB-MIP/TiO_2 and NIP/TiO_2 for RhB relative to Rh6G, respectively.

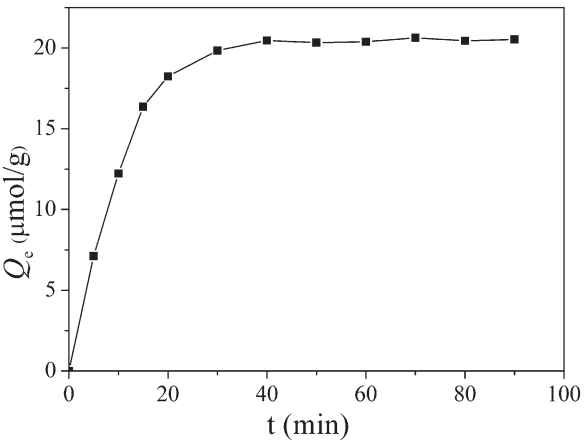

Figure 9. Adsorption kinetics curves of RhB-MIP/TiO_2.

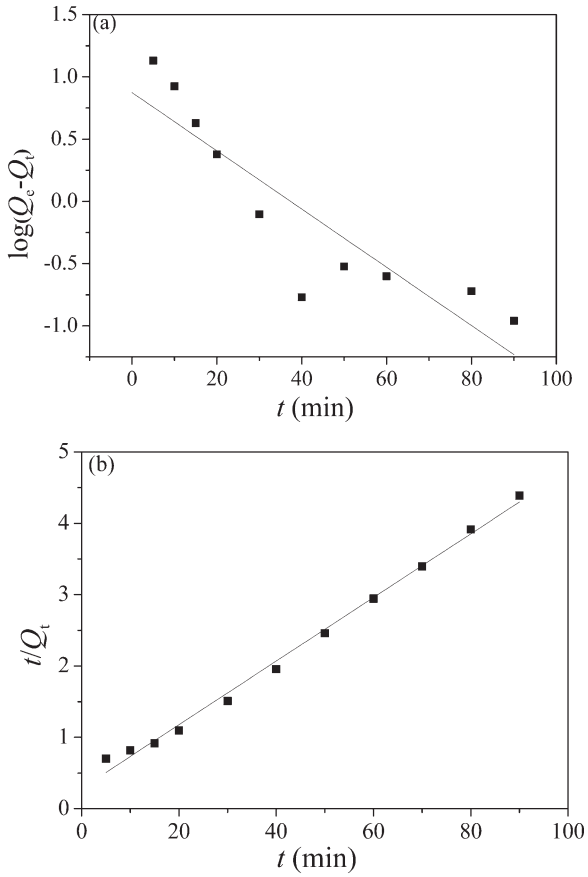

Figure 10. Pseudo-first-order kinetics (a) and pseudo-second-order kinetics (b) for adsorption of RhB on RhB-MIP/TiO_2.

Photocatalytic Activity Measurement

Photocatalytic activities of the RhB-MIP/TiO_2 and NIP/TiO_2 photocatalyst were evaluated by photocatalytic degradation of RhB and Rh6G aqueous solution under UV light irradiation, respectively. During the experiment, a 300 W UV lamp with a 254 nm cutoff filter as the light source was immersed in the photoreactor. RhB-MIP/TiO_2 or NIP/TiO_2 photocatalyst (0.1 g) were dispersed into RhB solution (100 mL, 10 mg L^{-1}), respectively. After the suspension was stirred for 40 min in dark to reach adsorption–desorption equilibrium, the concentration of the RhB solution was determined as the initial concentration

Table I. Adsorption Kinetics Constants for the Pseudo-First-Order Kinetics and Pseudo-Second-Order Kinetics

Constants	Pseudo-first-order kinetics	Constants	Pseudo-second-order kinetics
$Q_{e,c}$ [a] (μmol/g)	7.48	$Q_{e,c}$ [a] (μmol/g)	22.44
$Q_{e,max}$ [b] (μmol/g)	20.63	$Q_{e,max}$ [b] (μmol/g)	20.63
k_1 (min^{-1})	0.0538	k_2 (g/(μmol·min))	0.0069
R^2 [c]	0.7845	R^2	0.9940

[a] $Q_{e,c}$ is the theoretical calculating value of equilibrium adsorbed amount.
[b] $Q_{e,max}$ is the experimental value of equilibrium adsorbed amount.
[c] R^2 is the correlation coefficient.

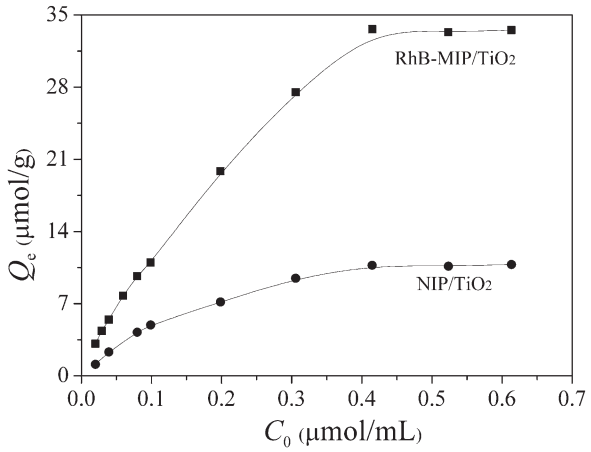

Figure 11. Adsorption isotherm curves of RhB-MIP/TiO_2 and NIP/TiO_2.

C_0, and then the photoirradiation started. During irradiation, about 4.0 mL of the suspension continually was taken from the reaction cell at given time intervals. The photocatalyst and the RhB solution were separated by centrifugation. The RhB concentration was analyzed through a UV–vis spectrophotometer at its characteristic wavelength. The degradation of Rh6G aqueous solution was tested by using the same method.

RESULTS AND DISCUSSION

Interaction Between RhB and AM

The principle of molecular imprinting lies in the preservation of the prepolymerized host–guest structure into a polymer matrix. MAA, 2-Vpy, and AM are widely used among the various functional monomers. The interactions between RhB and three functional monomers in ACN were studied by UV spectroscopic analysis, and the results are shown in Figure 3. It was clearly observed that the maximum absorbance of the mixture solutions was gradually declining from a to d, indicating the interaction between RhB and the functional monomers was gradually getting stronger. The functional monomer AM was chosen for the synthesis of the RhB-MIP/TiO_2 according to the experimental results. The interactions between AM and RhB were also studied at the molecular level via ^{1}H-NMR. Figure 4 shows the ^{1}H-NMR spectra of: (a) RhB, (b) AM, (c) RhB+AM in CD_3CN, respectively. It can be observed the upfield shift to about 9.58 of proton of —COOH in RhB and the shift of H ($\delta = 6.07$) of $-NH_2$ in AM when mixing RhB with AM. The spectra indicated that the epoxy group and a carboxyl group of RhB can interact with amide group of AM via the hydrogen bonds to form a stable host–guest complex. The interaction between RhB and AM is illustrated in Figure 1.

Table II. Adsorption Isotherm parameters for RhB-MIP/TiO_2 and NIP/TiO_2

Absorption isotherm models	Parameter	RhB-MIP/TiO_2	NIP/TiO_2
Langmuir isotherm model	R^2	0.9861	0.9904
	b (g/mL)	3.431	5.014
	[a] $Q_{m,c}$ (μmol/g)	53.19	14.95
Freundich isotherm model	R^2	0.9600	0.9494
	K_f (μmol/g)	71.99	23.40
	n	1.314	1.392

[a] $Q_{m,c}$ is the theoretical calculating value of maximum adsorbed amount

In order to further study the molar ratio of the template RhB and functional monomer AM, spectroscopic method was also used. Figure 5 shows the absorption spectra of the RhB in the presence of various concentration of AM in ACN. It can be seen from Figure 5 that the maximum absorbance of the mixture solutions was gradually declining with the concentration of AM increasing. The results indicated that the interaction between RhB and AM was getting stronger with the concentration of AM increasing further. However, excessive assembly of functional monomers may lead to nonfunctional monomer residues and their own association, which can increase the nonselective binding sites and decrease selective binding sites, respectively. So the molar ratio of the RhB and AM 1 : 4 was chosen for the synthesis of the RhB-MIP/TiO_2.

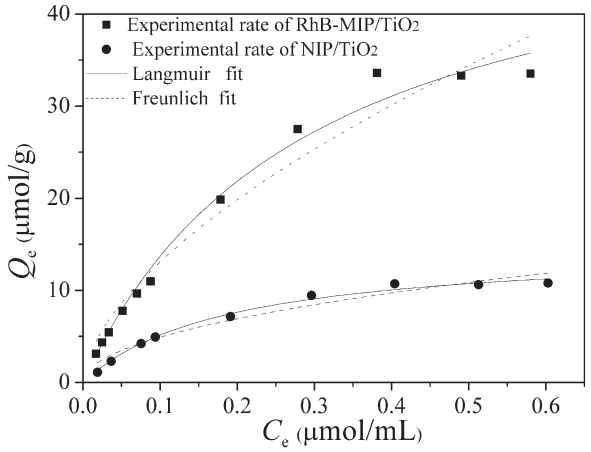

Figure 12. Langmuir and Freundlich isotherm models for RhB on RhB-MIP/TiO_2 and NIP/TiO_2.

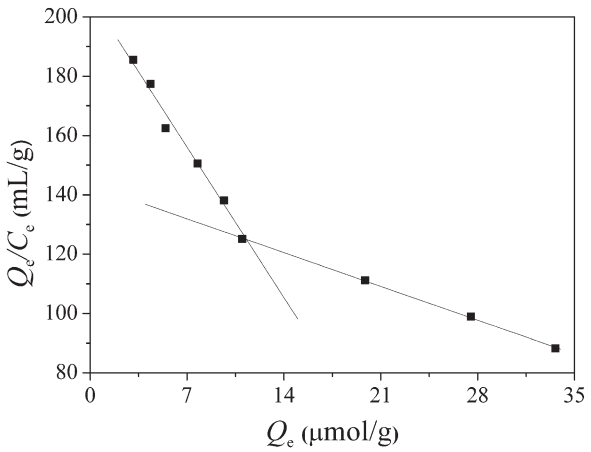

Figure 13. Scatchard analysis of RhB-MIP/TiO_2 for RhB.

Table III. The Results of the Scatchard Analysis

Binding site	Linear equation	K_d (μmol/mL)	Q_{max} (μmol/g)
Higher affinity site	$Q_e/C_e = -7.248Q_e + 206.8$ (R^2=0.9713)	0.1379	28.52
Lower affinity site	$Q_e/C_e = -1.627Q_e + 143.3$ (R^2 = 0.9992)	0.6146	88.07

Characteristics of RhB-MIP/TiO_2

The FTIR spectra of TiO_2, MPS-TiO_2, RhB-MIP/TiO_2, and NIP/TiO_2 are shown in Figure 6. In comparison to TiO_2, the spectrum of MPS-TiO_2 shows the new bands at 1719 cm^{-1}, 2953 cm^{-1}, and 1637 cm^{-1}, which are attributed to the stretching vibration absorption of C═O, C─H, and C═C, respectively. The infrared data indicated that KH-570 had been grafted successfully onto the surface of TiO_2. In addition, the spectra of RhB-MIP/TiO_2 and NIP/TiO_2 show that the stretching vibration absorption of saturated C─H band and carbonyl C═O in ester groups are strengthened distinctly, which resulted from polymerization crosslinking process. This observation reveals that the polymerization had been successfully carried out. The spectra of RhB-MIP/TiO_2 and NIP/TiO_2 show similar locations and appearances of the major bonds, which means that no template molecules were retained on the RhB-MIP/TiO_2.

The SEM image of TiO_2 and RhB-MIP/TiO_2 are given in Figure 7(a,b), respectively. It can be confirmed that TiO_2 was well dispersed in a spherical shape with bare surfaces. Compared with TiO_2, the surface of RhB-MIP/TiO_2 was rough and ruleless, it can be attributed to the coating by the products from the crosslinking reaction.

XRD patterns of the TiO_2 and RhB-MIP/TiO_2 photocatalysts are shown in Figure 8. In comparison with TiO_2, RhB-MIP/TiO_2 has no new diffraction peaks in the XRD pattern due to the amorphous imprinted layer. The average crystallite size of each sample is estimated by using the Scherrer formula, which is defined by eq. (7).

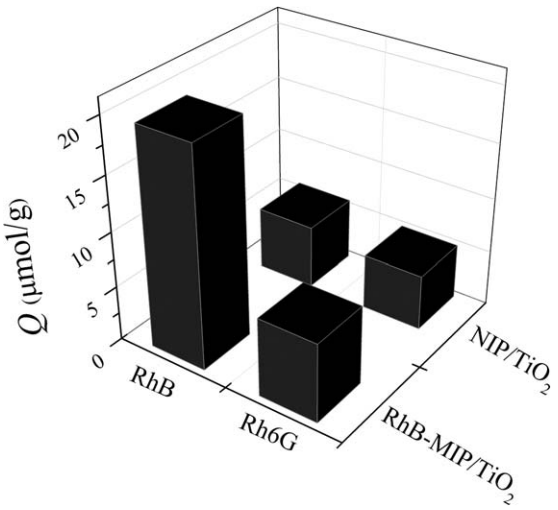

Figure 14. Adsorbed amounts of RhB-MIP/TiO_2 and NIP/TiO_2 for RhB and Rh6G, respectively.

$$D_{\text{Scherrer}} = \frac{K\lambda}{\beta\cos\theta} \quad (7)$$

where K is the Scherrer constant ($K = 0.89$), λ is the wavelength of the X-ray radiation ($\lambda = 0.154056$ nm), β is the line width at half-maximum height of the most intense peak, and θ is the diffraction angle.

The mean size of TiO_2 and RhB-MIP/TiO_2 photocatalysts can be estimated to be 17 nm and 23 nm, respectively. The result indicates that size of RhB-MIP/TiO_2 is larger than that of TiO_2. It can be attributed to the imprinted layer which coats on the surface of TiO_2.

Adsorption Kinetics

Adsorption kinetics curves of RhB-MIP/TiO_2 for RhB is presented in Figure 9. It can be seen that adsorbed amount of RhB-MIP/TiO_2 was observed to increase quickly with time in the first 25 min, and then the rate of adsorption increased slowly with time extension. After about 40 min, adsorption process reached equilibrium. It is reasonable to assume that the imprinted layer containing plentiful imprinted cavities was only on the surface of RhB-MIP/TiO_2, the template RhB can easily enter into the cavities and bind with the recognition sites. After the recognition sites were filled up with the template RhB, the diffusion resistance would lead to making the molecules enter into the inner cavities and bind with the recognition sites difficult, the rate of adsorption drops obviously and adsorption process achieved equilibrium gradually. In the current study, RhB-MIP/TiO_2 possessed good site accessibility and fast adsorption rate for RhB.

In order to further elucidate the uptake rate of adsorbate and potential rate-controlling step, the experimental data were analyzed by the pseudo-first-order kinetics [eq. (8)] and pseudo-second-order kinetics [eq. (9)], respectively.

$$\log(Q_e - Q_t) = \log Q_e - \frac{k_1 t}{2.303} \quad (8)$$

$$\frac{1}{Q_t} = \frac{1}{k_2 Q_e^2} + \frac{t}{Q_e} \quad (9)$$

where Q_e (μmol/g) and Q_t (μmol/g) are the adsorbed amount at equilibrium and time t (min), respectively, k_1 (min^{-1}) and k_2 (g/(μmol min)) are pseudo-first-order and pseudo-second-order rate constants of adsorption, respectively.

Pseudo-first-order kinetics and pseudo-second-order kinetics for adsorption of RhB-MIP/TiO_2 for RhB are shown in Figure 10(a,b), respectively. As seen from Figure 10(a,b), the pseudo-second-order kinetics fitted the experimental data quite well for the adsorption of RhB-MIP/TiO_2 for RhB. The adsorption kinetics constants for the pseudo-first-order kinetics and pseudo-second-order kinetics are given in Table I. From the data shown in Table I, for RhB-MIP/TiO_2, the pseudo-second-order kinetics produced a higher linear regression correlation coefficient ($R^2 = 0.9940$) than that of the pseudo-first-order kinetics. Moreover, the calculated equilibrium adsorbed amount by RhB-MIP/TiO_2 is 22.44 μmol/g, which is consistent with the experimental data (20.63 μmol/g). The facts suggested that the adsorption behavior of RhB-MIP/TiO_2 for RhB follows the

Table IV. Distribution Coefficient and Selectivity Coefficient Data of RhB-MIP/TiO_2 and NIP/TiO_2

	K_D (mL/g)			
	RhB	Rh6G	α	α'
RhB-MIP/TiO_2	111.0	37.14	2.99	-
NIP/TiO_2	29.86	25.69	1.16	2.58

pseudo-second-order kinetics, and that the overall rate of the adsorption process appeared to be controlled by the chemisorption process.

Adsorption Isotherms

The binding ability of RhB-MIP/TiO_2 and NIP/TiO_2 for RhB were investigated with static equilibrium binding experiments. The adsorption isotherm curves of RhB-MIP/TiO_2 and NIP/TiO_2 was provided in Figure 11. As shown in Figure 11, the equilibrium adsorbed amount of RhB-MIP/TiO_2 and NIP/TiO_2 increased gradually with initial solution, after a certain concentration, the adsorption reached saturation. In addition, it also could be found that the difference of adsorption amounts between RhB-MIP/TiO_2 and NIP/TiO_2 was getting larger with the increasing concentrition of the RhB. RhB-MIP/TiO_2 exhibited higher adsorption capacity than that of NIP/TiO_2 at either low or high concentration. The results suggested that RhB-MIP/TiO_2 and NIP/TiO_2 with almost the same element were remarkably different in their space-structure. The nonselective physical adsorption occurred between NIP/TiO_2 and RhB. In contrast, the RhB-MIP/TiO_2 adsorbed much more RhB than that of NIP/TiO_2 because a layer of imprinted material containing recognition sites was only on the surface of RhB-MIP/TiO_2.

To further characterize the adsorption behavior of RhB-MIP/TiO_2 and NIP/TiO_2, the equilibrium data of RhB-MIP/TiO_2 and NIP/TiO_2 were then fitted to the Langmuir [eq. (10)] and Freundlich [eq. (11)] isotherm models.

$$Q_e = \frac{Q_m b C_e}{bC_e + 1} \tag{10}$$

$$Q_e = K_f C_e^{1/n} \tag{11}$$

where Q_{max} (μmol/g) is the apparent maximum adsorbed amount, C_e (μmol/mL) is the equilibrium concentration, b (g/mL) is the adsorption equilibrium constant of Langmuir, K_f (μmol/g) is an indicative constant for the adsorption capacity of the sorbent and the constant $1/n$ indicates the intensity of the adsorption. A value of $1/n$ is less than 1.0 describing a favorable adsorption conditions.

Table V. Thermodynamic Parameters for the Adsorption of RhB Onto RhB-MIP/TiO_2 and NIP/TiO_2

	ΔH^θ	ΔS^θ	ΔG (kJ/mol)		
Polymer	(kJ/mol)	(J/(mol·K))	293 K	298 K	303 K
RhB-MIP/TiO_2	12.97	79.94	−10.45	−10.85	−11.25
NIP/TiO_2	11.25	64.84	−7.748	−8.072	−8.397

Figure 12 shows Langmuir and Freundlich isotherm models for RhB adsorption onto RhB-MIP/TiO_2 and NIP/TiO_2. It can be seen from Figure 12 that the Langmuir isotherm model fitted the experimental data significantly better than that of the Freundlich isotherm model. The adsorption isotherm parameters of RhB-MIP/TiO_2 and NIP/TiO_2 are listed in Table II. The values of the correlation coefficients for RhB-MIP/TiO_2 ($R^2 = 0.9861$) and NIP/TiO_2 ($R^2 = 0.9904$) by the Langmuir isotherm model were higher than those calculated by the Freundlich isotherm model, which indicates that RhB-MIP/TiO_2 and NIP/TiO_2 had better applicability for the Langmuir isotherm model. The results show that the value of $1/n$ is less than 1.0 indicating that RhB was favorably adsorbed onto RhB-MIP/TiO_2 and NIP/TiO_2.

The binding parameters of MIPs are mainly estimated by Scatchard analysis. Figure 13 shows the Scatchard analysis of RhB-MIP/TiO_2 for RhB. As seen in this figure, there were two distinct linear sections in the plot suggesting that two types of binding sites existed in the imprinted layer in respect to the adsorption for RhB: one is of high selectivity or affinity with a high binding energy, and the other is of low affinity with a low binding energy. The K_d and Q_{max} values were calculated from the slopes and intercepts of the two straight lines of the Scatchard plot, and the results are listed in Table III.

Selectivity Study

Figure 14 shows the adsorbed amounts of RhB-MIP/TiO_2 and NIP/TiO_2 for RhB and Rh6G, respectively. It can be seen that RhB-MIP/TiO_2 show a significantly higher adsorption capacity for RhB than that for Rh6G, whereas the absorbed amount of NIP/TiO_2 for the two substrates was almost the same. This indicated that the imprinted cavities have been created in RhB-MIP/TiO_2 owing to the addition of template molecule during polymerization, the adsorption ability of RhB-MIP/TiO_2 for RhB is far stronger than that for Rh6G. Table IV shows values of distribution coefficient (K_D), selectivity coefficient (α), and the relative selectivity coefficient (α'). From the data shown in Table IV, the selectivity coefficient of RhB-MIP/TiO_2 for RhB relative to Rh6G (2.99) is higher than that of NIP/TiO_2 for RhB relative to Rh6G (1.16). This implies that the RhB-MIP/TiO_2 had high adsorption selectivity for RhB over the structurally similar compounds Rh6G. The relative selectivity coefficient of RhB-MIP/TiO_2 for RhB relative to Rh6G is 2.58, which is greater than 1 and indicated the RhB-MIP/TiO_2 had higher adsorption selectivity than that of the NIP/TiO_2.

Adsorption Thermodynamics

Thermodynamic parameters, such as the changes in the Gibbs free energy (ΔG), enthalpy (ΔH^0), and entropy (ΔS^0), was calculated with the eqs. (12) and (13).

$$\ln\left(\frac{Q_e}{C_e}\right) = \frac{\Delta S^\theta}{R} - \frac{\Delta H^\theta}{RT} \tag{12}$$

$$\Delta G = \Delta H^\theta - T\Delta S^\theta \tag{13}$$

where Q_e (μmol/g) is the equilibrium adsorbed amount, C_e (μmol/mL) is the equilibrium concentration, T (K) is the absolute temperature, R (8.314 J mol^{-1} K^{-1}) is the ideal gas constant, ΔH^0 and ΔS^0 were obtained from the slope and intercept

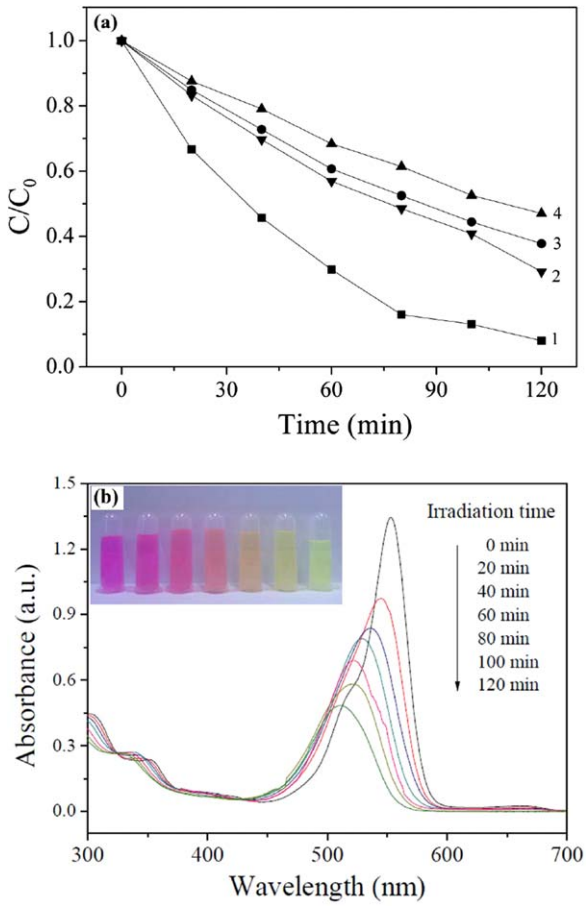

Figure 15. (a) The photocatalytic degradation of RhB over RhB-MIP/TiO_2 (1) and NIP/TiO_2 (2), respectively, Rh6G over RhB-MIP/TiO_2 (3) and NIP/TiO_2 (4), respectively. (b)Temporal UV–vis adsorption spectral changes during the photocatalytic degradation of RhB-MIP/TiO_2 toward RhB. [Color figure can be viewed in the online issue, which is available at wileyonlinelibrary.com.]

of the line plotted by $\ln(Q_e/C_e)$ versus $1/T$, respectively. The obtained thermodynamic parameters for RhB-MIP/TiO_2 and NIP/TiO_2 are listed in Table V.

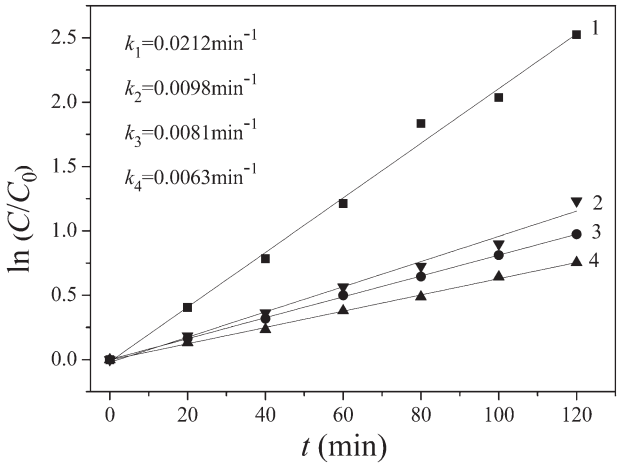

Figure 16. The apparent rate constant of RhB over RhB-MIP/TiO_2 (1) and NIP/TiO_2 (2), respectively, and Rh6G over RhB-MIP/TiO_2 (3) and NIP/TiO_2 (4), respectively

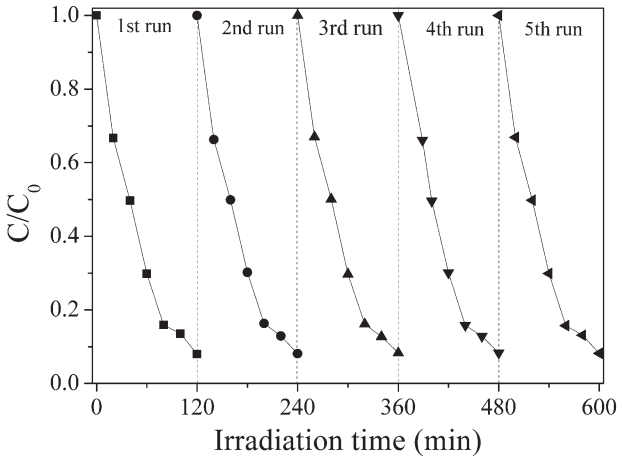

Figure 17. Results of cycling runs of RhB degradation over RhB-MIP/TiO_2.

As shown in Table V, the values of ΔG within the temperature range evaluated are negative, indicating that the adsorption of RhB-MIP/TiO_2 for RhB was spontaneous. The positive values of ΔS^0 suggested increased randomness at the solid–solution interface during the adsorption of RhB onto RhB-MIP/TiO_2. The positive values of ΔH^0 further confirmed the endothermic nature of the processes, so the increasing temperature caused more favorable adsorption of RhB onto RhB-MIP/TiO_2.

Photodegradation Activity

The photocatalytic activity of the RhB-MIP/TiO_2 and NIP/TiO_2 photocatalysts was measured by the degradation of RhB and Rh6G solution under UV light irradiation. As shown in Figure 15(a), the RhB-MIP/TiO_2 photocatalysts exhibits the highest photocatalytic activity toward RhB. The degradation efficiency reaches 92% after 120 min irradiation compared to 62% for Rh6G, respectively. The degradation efficiency of NIP/TiO_2 toward RhB and Rh6G is 70% and 53%, respectively. Figure 15(b) shows the time-dependent absorption spectra of RhB solution in the presence of RhB-MIP/TiO_2 microspheres. The maximum absorption of RhB suspension shifts from 553 to 511 nm. Meanwhile, it can be seen obviously that the color of the RhB solution changes gradually from fuchsia to colorless after irradiation for 120 min. The wavelength shift depicted is caused by deethylation of RhB because of attack by one of the active oxygen species on the *N*-ethyl group. The RhB dye was photodegraded into four intermediates [*N*,*N*-diethyl-*N*′-ethylrhodamine (DER), *N*,*N*-diethylrohodamine (DR), *N*-ethyl-*N*′-ethylrhodamine (EER), and Nethylrhodamine (ER)]. The ethyl groups in the RhB structure are removed one by one, and finally transformed into Rhodamine (R). Then, RhB and the intermediates are degraded completely.[33]

Figure 16 gives the kinetic rate for the photodegradation of RhB and Rh6G over different photocatalysts in the single systems, which clearly show that all the degradation processes follow a pseudo-first-order kinetics, which was defined by eq. (14).

$$\ln\left(\frac{C_0}{C}\right) = kt \tag{14}$$

where C_0 (mg/L) is the concentration of RhB and Rh6G at $t = 0$ (min), C (mg/L) is the concentration of RhB or Rh6G at instant t (min), and k (min^{-1}) is the apparent rate constant.

The values of the apparent rate constant (k) of the pseudo-first-order kinetics are also listed in Figure 16. The k value of the target RhB over RhB-MIP/TiO_2 is 0.0212 min^{-1}, being 216% of that over NIP/TiO_2 (0.0098 min^{-1}). The k value of Rh6G over RhB-MIP/TiO_2 is 0.0081 min^{-1}, being only 38% of that over RhB-MIP/TiO_2. Moreover, the differences of the k values for the photodegradation of RhB and Rh6G over NIP/TiO_2 are small. Compared with NIP/TiO_2, RhB-MIP/TiO_2 exhibited higher photocatalytic selectivity toward RhB. The adsorption capacity has much influence on the degradation behavior of organic pollutants, so this photocatalytic selectivity can be attributed to molecularly selective adsorption on the MIP coatings.

The reusability of RhB-MIP/TiO_2 by the cycling runs for RhB photodegradation was evaluated by using the same imprinted photocatalyst. The degradation results were shown in Figure 17. It can be seen from Figure 17 that the degradation ratios of RhB were almost kept stable around 92%. The photocatalytic activity does not obviously decline in RhB degradation after five recycling runs. Therefore, it can be inferred that the RhB-MIP/TiO_2 has high reusability.

Photocatalytic Mechanism of RhB-MIP/TiO_2

In general, the photocatalytic degradation process is mainly divided into two steps: the pollutants are first adsorbed on the surface of photocatalysts, and then the pollutants are degraded. For this reason, the mechanism of the photocatalytic degradation of RhB over the RhB-MIP/TiO_2 nanocomposites was proposed. At first, the RhB molecules can be adsorbed onto the imprinted layer of RhB-MIP/TiO_2 to form a moderately stable complex. When the RhB-MIP/TiO_2 nanocomposites are illuminated under the excitation of UV light, TiO_2 nanoparticles can absorb light and generate electron/hole pairs. The photo-generated electrons (e^-) migrate easily to the catalysts surface to react with oxygen to generate superoxide radicals ($\cdot O_2^-$), and the positive charged holes (h^+) can react with OH^- or H_2O to yield hydroxyl radicals ($\cdot OH$). The resulting radicals are powerful enough to decompose oxidized RhB to the degradation products. The whole process can be clearly described as eqs. (15–20).

$$\text{RhB-MIP/TiO}_2 + \text{RhB} \xrightarrow{\text{adsorption}} \text{RhB-MIP/TiO}_2\text{-RhB} \quad (15)$$

$$\text{RhB-MIP/TiO}_2 \xrightarrow{h\nu} \text{RhB-MIP/TiO}_2(h^+ + e^-) \quad (16)$$

$$e^- + O_2 \rightarrow \cdot O_2^- \quad (17)$$

$$H_2O + h^+ \rightarrow \cdot OH + H^+ \quad (18)$$

$$OH^- + h^+ \rightarrow \cdot OH \quad (19)$$

$$\cdot OH + \text{RhB} \rightarrow \text{Degration products} \quad (20)$$

CONCLUSIONS

In this study, a highly selective photocatalyst RhB-MIP/TiO_2 was successfully prepared by surface imprinting technique with RhB as template. Batch mode binding experiments revealed that the RhB-MIP/TiO_2 possessed strong affinity for the template RhB, and displayed high special adsorption capacity, excellent site accessibility, and significantly good mass transport property. The equilibrium adsorption data of RhB-MIP/TiO_2 for RhB can be well fitted by the Langmuir isotherm model, and the kinetics property of RhB-MIP/TiO_2 was well characterized by the pseudo-second-order kinetics. The selectivity experimental results show that the RhB-MIP/TiO_2 exhibited higher recognition selectivity and binding affinity for the template RhB. The RhB-MIP/TiO_2 also displayed higher photocatalytic selectivity than that of NIP/TiO_2.

REFERENCES

1. Ansari, R.; Keivani, M. B.; Delavar, A. F. *J. Appl. Polym. Sci.* **2011**, *122*, 804.
2. Gao, H. J.; Wang, J.; Zheng, L. Q. *Chem. Eng. J.* **2013**, *234*, 372.
3. Safavi, A.; Momeni, S. *J. Hazard. Mater.* **2012**, *201–202*, 125.
4. Zahrim, A. Y.; Hilal, N. *Water Resour. Res.* **2013**, *3*, 23.
5. Zhu, M. X.; Lee, L.; Wang, H. H.; Wang, Z. *J. Hazard. Mater.* **2007**, *149*, 735.
6. Zheng, Y. P.; Yao, G. H.; Cheng, Q. B.; Yu, S. C.; Liu, M. H.; Gao, C. *J. Desalination* **2013**, *328*, 42.
7. Makhoukhi, B.; Moulessehoul, H.; Azzouz, A.; Villemin, D. *Appl. Clay Sci.* **2010**, *50*, 354.
8. Chan, L. S.; Cheung, W. H.; McKay, G. *Desalination* **2008**, *218*, 304.
9. Sun, J.; Yan, X.; Lv, K. L.; Sun, S.; Deng, K. J.; Du, D. Y. *J. Mol. Catal. A: Chem.* **2013**, *367*, 31.
10. Pelaez, M.; Baruwati, B.; Varma, R. S; Luque, R.; Dionysiou, D. D. *Chem. Commun.* **2013**, *49*, 10118.
11. Yang, C.; Tian, L.; Ye, L.; Peng, T. Y.; Deng, K. J.; Zan, L. *J. Appl. Polym. Sci* **2011**, *120*, 2048.
12. Deng, F.; Li, Y. X.; Luo, X. B.; Yang, L. X.; Tu, X. M. *Colloids Surf. A: Physicochem. Eng. Asp.* **2012**, *395*, 183.
13. Zhang, G.; Choi, W. Y.; Kim, S. H.; Hong, S. B. *J. Hazard. Mater.* **2011**, *188*, 198.
14. Miyayama, S.; Nishijima, K.; Kamai, T.; Chiyoya, T.; Tsubota, T.; Ohno, T. *Sep. Purif. Technol.* **2007**, *58*, 206.
15. Inumaru, K.; Murashima, M.; Kasahara, T.; Yamanaka, S. *Appl. Catal. B: Environ.* **2004**, *52*, 275.
16. Damin, A.; Labres, I.; Xamena, F. X. L.; Lamberti, C.; Zecchina, A. *J. Phys. Chem. B* **2004**, *108*, 1328.
17. Shen, X. T.; Zhu, L. H.; Li, J.; Tang, H. Q. *Chem. Commun.* **2007**, *11*, 1163.
18. Zhou, H.; Xu, Y. P.; Tong, H. W.; Liu, Y. X.; Han, F.; Yan, X. Y.; Liu, S. M. *J. Appl. Polym. Sci.***2013**, *128*, 3846.
19. Rezaei B.; Rahmanian O. *J. Appl. Polym. Sci.* **2012**, *125*, 798.
20. Luo, X. B.; Deng, F.; Luo, S. L.; Tu, X. M.; Yang, L.X. *J. Appl. Polym. Sci.* **2011**, *121*, 1930.
21. He, M. Q.; Song, C. C.; Yan, Y. S.; Chen, Y.Q.; Wan, J. C. *J. Appl. Polym. Sci.* **2011**, *121*, 2354.
22. Zhang, X. J.; Xu, Z. L.; Feng, J. L.; Bing, N. C.; Yang Z. G. *J. Membr. Sci.* **2008**, *313*, 97.

23. Xie, J. Q.; Cai, C. Q.; Yang, H.; Chen, X. *Anal. Lett.* **2013**, *46*, 107.
24. Duan, Z. J.; Yi, J. H.; Fang, G. Z.; Fan, L. P.; Wang, S. *Food Chem.* **2003**, *139*, 274.
25. Shen, X. T.; Zhu, L. H.; Liu, G. X.; Yu, H. W.; Tang, H. Q. *Environ. Sci. Technol.* **2008**, *42*, 1687.
26. Zhao, P. N.; Hao, J. C. *Food Chem.* **2013**, *139*, 1001.
27. Xu, X. Z.; Chen, S. X.; Wu, Q. H. *J. Colloid Interface Sci.* **2012**, *385*, 193.
28. Lu, N.; Chen, S.; Wang, H. T.; Quan, X.; Zhao, H. M. *J. Solid State Chem.* **2008**, *181*, 2852.
29. Li, Y.; Yin, X. F.; Chen, F. R.; Yang, H. H.; Zhuang, Z. X.; Wang, X. R.; *Macromolecules* **2006**, *39*, 4497.
30. Zhang, L.; Nie, Y.; Hu, C.; Qu, J. *Appl. Catal. B: Environ.* **2012**, *125*, 418.
31. Li, T.; Zhao, L.; He, Y.; Cai, J.; Luo, M.; Lin, *J. Appl. Catal. B: Environ.* **2013**, *129*, 255.
32. Zhu, L.; Ghosh, T.; Park, C. Y.; Meng, Z. D.; Oh, W. C. *Chin. J. Catal.* **2012**, *33*, 1276.
33. Xu, H.; Li, H. M.; Sun, G. S.; Xia, J. X.; Wu, C. D.; Ye, Z. X.; Zhang, Q. *Chem. Eng. J.* **2010**,*160*, 33.